Dept. of Earth and Environmental Sciences, Tulane University
Dissertation Prospectus

1. Summary

Allogenic (external) tectonic and climatic forcings can create signals, such as changes in sediment flux, Q_s, that travel through the sediment routing system to eventually become encoded as strata in the rock record. These signals, however, may become buffered or shredded by autogenic (internal) processes of sediment transport, deposition, and remobilization. Buffering is the muting of a signal when the exogenic forcing acts over a timescale shorter than the landscape's response time (RT, the time a landscape takes to completely adjust to a new boundary condition) (Allen, 2008; Straub et al., 2020). Shredding occurs when autogenic stochastic processes rework a signal such that it can no longer be reconstructed (Jerolmack and Paola, 2010; Straub et al., 2020). Understanding the effects of autogenic processes on the erosion, transport, and deposition of sediment is essential for interpreting paleo-tectonics and paleo-climate from stratigraphy.

Recent studies of signal propagation have fallen into two broad categories: those studying signal shredding by stochastic autogenic processes (e.g., Jerolmack and Paola, 2010; Pizzuto et al., 2017; Griffin et al., 2023), and those studying buffering by deterministic fluvial networks (e.g., Castelltort and Van Den Driessche, 2003; Godard et al., 2013; Li et al., 2018; Sharman et al., 2019). Using different modeling approaches, Jerolmack and Paola (2010), Pizzuto et al. (2017), and Griffin et al. (2023) show that although autogenic storage and release of sediment shreds short-term signals, long-term signals may remain partially preserved. Theory developed from field and laboratory measurements suggests that the transport of mass over the Earth's surface is noisy, but that over some timescales this noise has structure (Jerolmack and Paola, 2010). Specifically, it is theorized that a key timescale exists (T_{RW}) that separates correlated (red) from uncorrelated (white) noise, below which propagating environmental signals get significantly degraded (Griffin et al., 2023). Li et al. (2018) explored the time lag (buffering) effect of a dendritic fluvial network using a detachment-limited stream power model in which no sediment storage is possible. Despite the lack of autogenic processes, the fluvial network did not produce a detectable signal for any rock uplift pulse shorter than 25% of the catchment's RT. With a similar model, Godard et al. (2013) found that the frequency of periodic precipitation forcing altered the amplitude of a sediment flux (Q_s) signal at the outlet, with a specific period maximizing the signal strength. Notably, none of the buffering models consider the stochastic processes brought up by the shredding models and vice versa.

For my dissertation, I bridge the gap by applying a stochastic process to a 2D sediment transport network. I couple stochastic landsliding and fluvial processes in a numerical landscape evolution model (LEM) and explore the questions: How do the stochastic fluxes of sediment from hillslopes interact with the buffering effects of a fluvial network to shred or preserve tectonic signals? Does the coupled system have a timescale T_{RW}, and if so, what causes that noise transition? I also use physical avalanching rice pile and delta experiments to investigate: Does noisy sediment input change the autogenic behaviour of stochastic mass flux systems? What noise signatures and timescales transfer from one domain of the sediment routing system to the next?

Project 1

In Project 1, I use a LEM to explore how stochastic landsliding affects steady-state erosional catchments with regard to morphology, dynamics, and sediment delivery. The LEM is constructed using the Landlab modeling toolkit, an open-source Python environment for modeling planetary surface processes (Hobley et al., 2017; Barnhart et al., 2020). I couple four process components: *SpaceLargeScaleEroder* to model fluvial incision, transport, and deposition, *ExponentialWeatherer* to model bedrock weathering, *DepthDependentDiffuser* to model hillslope sediment transport, and *BedrockLandslider* to model stochastic landsliding (Shobe et al., 2017; Barnhart et al., 2019; and Campforts et al., 2020, respectively). I measure Q_s at the outlet and apply the multi-taper method of spectral analysis to determine what noise spectra exist over various timescales. From this, I find the transition timescales (e.g., T_{RW}) and relate them quantitatively to the processes governing sediment transport. I explore the effects of catchment drainage area and variations in three model parameters: landslide return time (t_{LS}), erodibility (K_{sed}) of the landslide deposits, and settling velocity (v_s) of fluvially entrained sediment. All experiments use a constant uplift rate of 1 mm/yr. Timeseries analysis begins only once the synthetic landscape has reached a dynamic equilibrium. Thus, the results describe only the steady-state behaviour of the system.

Preliminary results show that, similar to the avalanching rice pile experiments (Jerolmack and Paola, 2010; Griffin et al., 2023), the system generates noisy output Q_s from a steady input. The power spectra show a T_{RW} at timescales in the range of 10^3-10^5 years, depending on the parameters. T_{RW} scales with the residence time of landslide deposits as fluvial incision generates correlation in Q_s (red noise) while eroding the deposits.

The landscape morphology reflects the stronger of the two erosive processes. When t_{LS} is high, landslides occur infrequently, so bedrock is primarily eroded by fluvial incision, resulting in short hillslopes, high drainage density, and a relatively tortuous river network. When t_{LS} is low, the landscape is dominated by long, planar hillslopes caused by frequent landsliding. The river network is short and has a low drainage density, channel steepness is high, and relief is high as the fluvial system uses the majority of its erosive power to evacuate sediment generated by landslides. When the two processes are balanced, the landscape becomes highly dynamic as local erosive dominance shifts temporarily between the two processes.

Project 2

In Project 2, I add exogenic forcing to the LEM to explore shredding and propagation of sedimentary signals that are generated in these catchments. I add a tectonic signal by generating pulses lasting as long as the timescale T_{RW} during which uplift rate is increased tenfold. Between pulses, uplift rate is returned to baseline for the same duration. I then vary the magnitude and periodicity of the pulses to explore the signal shredding capabilities of stochastic landsliding. In addition, I add a magnetic susceptibility (χ) tracker to the model, allowing me to compare numerical results to field χ measurements from a study site in Sicily. χ tends to be enhanced in soil eluvial horizons compared to the subsoil and parent bedrock material (Le Borgne, 1955; Thompson and Oldfield, 1986) due to pedogenesis (Lu et al., 2012) and preferential accumulation of weathering-resistant magnetic minerals (Singer, 1996). Surficial landslides composed mostly of soil should therefore provide sediment with a high χ signal to the fluvial system while bedrock exhumed by deep-seated landslides should dilute the χ

signal. As χ is related to the sediment's chemical composition rather than its volumetric flux, it may tell a different story than Q_s.

Based on the work of Griffin et al., 2023, I hypothesize that tectonic pulses of all magnitudes that have periodicity longer than T_{RW} will be detectable as a spike in the Q_s power spectra. Those with periods shorter than T_{RW} will generate significantly degraded signals. I expect that high amplitude signals may be detectable at all timescales, but low amplitude signals may not be detectable at any timescale, as they will be masked by autogenic noise. Additionally, I hypothesize that χ may carry signals from different events and over different timescales than Q_s. The transient response of landscape relief to external forcing may generate χ signals over timescales of RT. As relief builds in response to increased rock uplift rates, the frequency of large deep-seated bedrock landslides should increase and cause a corresponding decrease in χ. On the other hand, relief decreases in response to decreasing rock uplift rates, which should lead to fewer bedrock landslides and a larger proportion of hillslope material coming from high-χ diffusive hillslope transport.

Project 3

In Project 3, I will use physical avalanching rice pile and delta experiments to investigate the effects of noisy delivery of sediment to stochastic mass flux systems. Research on the depositional domain tends to assume sediment delivery (Q_{in}) from upstream is steady or follows simple periodic oscillations (e.g., Jerolmack and Paola, 2010; Griffin et al., 2023; Foreman and Straub, 2017). This is unlike the sporadic and unsteady delivery that occurs in natural systems. I will explore how that noise transfers through the systems and interacts with the noise generated by mass transport within the systems. My rice pile experiments will test the timescales over which correlated noise entering a sediment transport segment can be transferred down system. Delta basin experiments will confirm whether the rice pile results can be generalized to other sediment transport systems.

I expect that correlation in noisy input Q_s will transfer to measurable correlation in output flux only at timescales longer than T_{RW}. Thus, in a particular sediment routing system, the process generating the longest timescale of correlation may dictate the timescales over which signals are preserved.

2. Timeline/Work Plan

Semester	**Project 1:** **LEM: steady state**	**Project 2:** **LEM: signal shredding**	**Project 3:** **Physical delta experiment**
Already complete	- Develop LEM - Run model scenarios	- Develop LEM - Develop χ model	
2023 – Fall	- Analyze results - Write Manuscript	- Design model scenarios - Run model scenarios	- Rice piles: design experiments
2024 – Spring	- Write Manuscript	- Analyze results	- Rice piles: run experiments - Delta: design, run experiment
2024 – Summer		- Write Manuscript	- Analyze results - Write manuscript
2024 – Fall	Defend	Defend	Defend

Collaborators

Project 1: Nicole Gasparini, Kyle Straub, Benjamin Campforts

Project 2: TESPRESSO members, Kyle Straub, Benjamin Campforts

Project 3: Nicole Gasparini, Kyle Straub, Chloe Griffin

3. Project 1

3.1 Introduction

The scientific community has a good understanding of how deterministic equations that simulate erosional and depositional processes such as stream power, hillslope diffusion, and bedrock weathering act and interact in an LEM (Willgoose et al., 1991; Tucker and Bras, 1998; Gasparini et al., 2007; Perron et al., 2009; Goren et al., 2014). However, the inclusion of stochastic processes in LEMs is less common (Densmore et al., 1998; Crave and Davy, 2000; Tucker and Bras, 2000) and the specific effects of stochastic landslides on landscape form and dynamics are only beginning to be explored (e.g., Campforts et al., 2020; Campforts et al., 2022). As well, to my knowledge, there has been no study of Q_s from LEMs containing a stochastic landsliding component. I address this knowledge gap by building on the concepts developed by others using numerical and physical avalanching sand and rice pile models (Hwa and Kardar, 1992; Jerolmack and Paola, 2010; Griffin et al., 2023). In these experiments, a steady feed of rice grains is added to the top of a pile, below which there is a weighing scale. As grains are added, the pile eventually oversteepens and an avalanche occurs, flowing down the pile to deposit on the scale. Jerolmack and Paola (2010) and Griffin et al. (2023) show that the noise generated by steady-state mass fluxes from stochastic rice pile avalanches is structured over certain timescales. Timescales shorter than the duration of a single failure event are characterized by correlation (or red noise) in mass flux as the avalanche deposits over time onto the scale. This correlation disappears at timescales longer than the longest failure event, where the red noise transitions to white (uncorrelated) noise. Marking the transition from red to white noise is the key timescale, T_{RW}. Power spectral analysis shows that propagating environmental signals get significantly degraded at timescales below T_{RW} (Griffin et al., 2023).

My first project establishes an understanding of the steady-state landscape and Q_s signatures generated by the numerical model. Beginning with a baseline model run, I characterize landscape metrics, dynamics, and processes, and analyze noise and structure in Q_s exiting the catchment. I then adjust parameters that determine landslide frequency (t_{LS}), landslide deposit erodibility (K_s), and fluvial sediment transport (through net effective settling velocity, V) to determine how each of these affects the steady-state landscape and the critical timescale of T_{RW}. From baseline understanding of these various dynamic equilibrium states, it is then possible to explore signal shredding and propagation by transient landscape response to external forcing (Project 2).

In this project, I answer the following questions. Does the coupled system have a timescale T_{RW}? If so, what processes generate correlation up to that timescale and which model parameters govern those processes? How do those model parameters affect the timescale T_{RW}?

3.2 Hypothesis

I hypothesize that the power spectra will show a characteristic shape similar to those of the Griffin et al. (2023) rice pile models, though with very different time scales. Correlation should be caused by fluvial erosion of landslide deposits and be dependent on landslide deposit volume, sediment erodibility, and sediment settling velocity. Reducing landslide frequency (t_{LS}) should generate larger landslides that deposit larger masses of sediment that take longer to erode, thus increasing the timescale for T_{RW}. Decreasing the erodibility of the landslide deposits (K_s) should increase the time to erode the deposits and therefore increase the timescale for T_{RW}. Increasing settling velocity (v_s) should lengthen the transport time for sediment to exit the catchment and therefore increase the timescale for T_{RW}. It is

possible that the increased complexity of the LEM compared to a 1D rice pile will also increase the complexity of the Q_s power spectra. For example, long-term drainage rearrangement may generate correlation over very long timescales.

3.3 Methods

The LEM couples three process components in Landlab: *SpaceLargeScaleEroder* to model fluvial incision, transport, and deposition, *DepthDependentDiffuser* to model hillslope sediment transport, and *BedrockLandslider* to model stochastic landsliding (Shobe et al., 2017; Barnhart et al., 2019; and Campforts et al., 2020, respectively).

Fluvial processes

SpaceLargeScaleEroder is a mass conservative erosion-deposition fluvial sediment transport model that tracks both bedrock and sediment mass (Shobe et al., 2017). Sediment entrainment and deposition are explicitly calculated, allowing direct calculation of Q_s and of alluvial layer thickness. The framework for conservation of mass states that the change in topographic surface elevation, η (units of length, L), over time is the sum of changes to bedrock elevation, R (L), and sediment layer thickness, H (L):

$$\frac{\partial \eta}{\partial t} = \frac{\partial R}{\partial t} + \frac{\partial H}{\partial t} \quad \text{(eq. 1)}$$

This can be expanded to include the processes driving those changes:

$$\frac{\partial \eta}{\partial t} = U - E_{r_{fluv}} + \left(\frac{D_{s_{fluv}} - E_{s_{fluv}}}{1 - \varphi_{sed}}\right) \quad \text{(eq. 2)}$$

Where U (L T^{-1}) is bedrock uplift rate, E_r is the erosion rate of bedrock, E_s is the erosion rate of sediment, D_s is the deposition rate of sediment (all L T^{-1}), and φ_{sed} (-) is sediment porosity. The subscript $fluv$ differentiates these fluvial erosion and deposition terms from their hillslope equivalents that are described below in the Landslides section.

Fluvial erosion of bedrock, $E_{r_{fluv}}$ (L T^{-1}), and sediment, $E_{s_{fluv}}$ (L T^{-1}), follow a unit stream power formulation modified by an erosional efficiency term that modulates the relative effectiveness of each process. As sediment thickness increases, covering more of the bedrock bed, erosion of that sediment increases exponentially while erosion of the underlying bedrock decreases by the same exponential function. Fluvial sediment deposition rate, $D_{s_{fluv}}$ (L T^{-1}), uses a volumetric sediment-to-water flux ratio and a net effective settling velocity parameter, which accounts for turbulence and determines sediment transport distance, following Davy and Lague (2009). A complete description of the component's mathematics is provided in Shobe et al. (2017).

Landslide processes

BedrockLandslider models stochastic discrete landslides using the Culmann criterion (e.g., Densmore et al., 1998). It simulates deep-seated gravity-driven landslides that simultaneously erode both bedrock and sediment. The component uses the same framework for conservation of mass as *SpaceLargeScaleEroder*, though the processes for erosion and deposition are different. When the components are combined, change in local elevation is calculated as follows:

$$\frac{\partial \eta}{\partial t} = U - E_{r_{fluv}} + \left(\frac{D_{s_{fluv}} - E_{s_{fluv}}}{1 - \varphi_{sed}}\right) - E_{r_{hill}} + \left(\frac{D_{s_{hill}} - E_{s_{hill}}}{1 - \varphi_{sed}}\right) \quad \text{(eq. 3)}$$

Where U (L T^{-1}) is rock uplift rate, φ_{sed} (-) is sediment porosity, and E and D are erosion and deposition rate (L T^{-1}), respectively. The subscripts *r* and *s* indicate bedrock and sediment, respectively, and the subscripts $hill$ and $fluv$ differentiate hillslope erosion and deposition terms from their fluvial equivalents. In the numerical calculations, the algorithm breaks up equation 3 into three sequential parts: it first adds rock uplift, then calculates fluvial erosion/deposition in response to the uplift, and finally calculates hillslope erosion/deposition in response to fluvial erosion.

Landslides are initiated at 'unstable' nodes, where topographic slope exceeds the angle of internal friction. Whether a landslide occurs at an 'unstable' node during a given timestep depends on the node's probability of landsliding, p_{LS}, and a stochastic sampling scheme. The landslide failure plane is defined by a dip angle that bisects local topographic slope and the angle of internal friction and extends upwards in all directions from the initial point of failure. All material (sediment and bedrock) that lies above the failure plane is eroded. Deposition occurs downslope of this point following a nonlinear and nonlocal deposition equation. Landslide-derived sediment travels over the landscape along a multiple-flow-direction path, causing spread-out deposition in proportion to local slope. A detailed description of the mathematics behind the component can be found in Campforts et al. (2020) and Campforts et al. (2022).

Hillslope processes

DepthDependentDiffuser models hillslope sediment transport by diffusive processes. I couple it with the *ExponentialWeatherer*, a bedrock weathering function that transforms bedrock into mobile regolith in the style of Ahnert (1976). Hillslope creep of this mobile sediment is modeled following a depth-dependent transport law based on the approaches of Johnstone and Hilley (2015) and Barnhart et al. (2019). I use the *DepthDependentDiffuser* and *ExponentialWeatherer* to control ridgetop morphology in cases when fluvial incision dominates and would produce unrealistically steep slopes.

Model domain

I first generate a base case model scenario and then vary three parameters to test their effects on the steady-state morphology and the critical timescale of T_{RW}: the net effective settling velocity (V) and the landslide deposit erodibility coefficient (K_s) in *SpaceLargeScaleEroder*, and the landslide return time (t_{LS}) in *BedrockLandslider*. The base case domain is composed of a synthetic 9.5 km long by 3.25 km wide grid of square cells with a spatial resolution of 50 m. The initial grid is seeded with randomly generated microtopography and allows drainage out of a single outlet point in the south-east corner. The temporal resolution is 10 years, and the total run time is 20 million years of dynamic steady state Q_s after model spin-up.

Table 1 shows the value for all model parameters for the base case scenario. These values are based approximately on measured values from the Pagliara watershed in northeastern Sicily, Italy. I use this real-world catchment as a guideline to ensure that the base case scenario reproduces realistic topography and erosion rates (Figure 2). There is no intention to replicate the exact morphology. The Pagliara River is 12 km long and drains an area of 27 km^2 with a total relief of 1,193 m (Pavano et al., 2016). The bedrock is predominantly composed of low-grade metamorphic pelites, arenites, phyllites, and schists (Lentini et al., 2000). Pavano et al. (2016) calculated a detachment-limited erosion coefficient (or K value) of 1.13 ± 0.02 x 10^{-5} m$^{0.14}$/ky and a Θ value (*m/n*) of 0.42 that produce a best fit to the stream power equation for the longitudinal profile. They calculated a rock uplift rate of 1.68 m/ky based on elevations of nearby dated marine terraces from Catalano and De Guidi (2003). Cyr et al. (2010)

calculated a catchment-averaged erosion rate of 0.97 ± 0.11 mm/yr over the past 125 ka using in situ cosmogenic Be^{10}.

For the base case scenario, K_s is set to 10^{-4} m^{-1} and V is set to 1 m/y. Landslide return time, t_{LS}, is set to 10^5 y such that the landslide frequency-area relationship matches well with those from studies of landsliding along normal fault bounded mountain ranges in the nearby Calabria, Campania, and Basilicata regions (Goswami et al., 2011; Roda-Boluda et al., 2018). I then set up 3 suites of model runs in which I vary V, K_s, and t_{LS}. Each suite is composed of 4 model runs: VS, S, L, and VL, in which the parameter is set to a 'very small', 'small', 'large', and 'very large' value compared to the base case (Table 2). In suite 1, I adjust t_{LS} by one order of magnitude for each run. In suite 2, I adjust K_s by a half order of magnitude for each run. In suite 3, I adjust V by one order of magnitude for each run.

Finally, I re-run the entire series of models on catchments of different size and shape to see whether these influence the noise structure. I use square catchments with sides of length 1 to 10 km (i.e., drainage areas of 1 to 100 km^2) to test the effects of catchment size. Then, to test the impact of mainstem channel length, I use rectangular catchments with width-to-length ratios of 1:4 for the same range of drainage areas.

Table 1. Model parameter values used in all model scenarios.

Parameter	Units	Value
# of rows	-	65
# of columns	-	190
Cell size	m	50
Timestep	yr	10
Run time	yr	20,000,000
U	mm yr^{-1}	1
W	mm yr^{-1}	1
φ_{sed}	-	0
K_r	m^{-1}	0.00001
m	-	0.5
n	-	1
Initial H	m	0
H^*	m	1
φ	degrees	35

Table 2. Model parameter values used in model run suites.

Parameter	Units	Value for model run				
		VS	S	Base	L	VL
t_{LS}	yr	10^3	10^4	10^5	10^6	10^7
K_s	m^{-1}	10^{-5}	50^{-5}	10^{-4}	50^{-4}	10^{-3}
V	m yr^{-1}	0.01	0.1	1	10	100

Spectral Analysis

I use the multi-taper method in the open-source RedConf package in MATLAB to generate spectral estimates of the timeseries of Q_s exiting the catchment for each experiment. These allow me to characterize the nature of the noise generated by landsliding. Prior to spectral analysis, I subtract the mean Q_s value from each data point to generate a timeseries of Q_s deviation from the mean.

The multi-taper method uses a series of orthogonal discrete prolate spheroidal sequences (DPSS) to taper the timeseries and averages the periodograms generated from each taper (Thomson, 1982; Weedon, 2003). This method produces a smoothed spectral estimation, making it easier to pick out statistically significant peaks. I apply five tapers and use no zero-padding. For visualization, I normalize each spectral estimate by dividing every power value by the sum of power in the spectral estimate. Relative power allows for easy comparison between timeseries.

3.4 Results

I have finished running all the scenarios for Project 1, I have not yet analyzed the effects of varying K_s or V. I intend to finish this analysis in the Fall 2023 semester. The following section describes results from the base-case scenario and the effects of landslide return time on the Q_s timeseries, Q_s power spectra, and landscape morphology.

Timeseries

Like avalanching rice pile experiments (Jerolmack and Paola, 2010; Griffin et al., 2023), the autogenic processes within the system generate noise in the output Q_s even though the input of material is steady (examples in Figure 2).

A small landslide return time, t_{LS}, causes a high frequency of landsliding, which results in rapid low magnitude Q_S fluctuations about the mean (Figure 2a). There are many landslides that occur throughout the catchment at the same time and there is little time for hillslopes to steepen enough that they generate extremely large events. A large t_{LS} causes a low frequency of landsliding, and results in less rapid and smaller magnitude fluctuations in Q_S (Figure 2c). Infrequent large near-instantaneous spikes in Q_S are evidence of the largest individual landslides that occur in this system. Landslides are infrequent enough that few events, if any, occur at the same time. For a moderate t_{LS} (Figure 2b), the internal dynamics of the system cause larger magnitude changes in Q_S than those produced by individual landslides. There is likely enough time between landslides for hillslopes to steepen such that large events may occur (not possible with a shorter t_{LS}), but events are frequent enough throughout the landscape that several occur at the same time to generate extreme pulses of sediment discharge to the outlet.

Spectral analysis

Despite their visual differences when plotted in time, the three timeseries shown in Figure 2 share some common attributes in their power spectral estimates (Figure 3). All three power spectra exhibit a red noise regime at small timescales that rolls over to white noise at longer timescales. This transition (T_{RW}) is clear for the high frequency landsliding scenario ($t_{LS} = 10^3$ y) and occurs at approximately 3,000 years. However, for the two longer-scale return times ($t_{LS} = 10^5$ y and $t_{LS} = 10^7$ y), T_{RW} is not sharp and is difficult to attribute to an exact timescale. I have marked the approximate middle of the transition in Figure 3 at 10,000 y for the moderate frequency scenario and 40,000 years for the low frequency scenario. T_{RW} seems to scale with the residence time of landslide deposits, as fluvial incision generates correlation in Q_s (red noise) while it erodes those deposits.

The high frequency landsliding scenario also exhibits a transition from white to blue noise (T_{WB}) and therefore follows the tripartite power spectrum framework described in Griffin (2023). For rice piles, T_{WB} represents a regeneration timescale, which is the time required for mass influx to replenish the mass lost in the largest failure event. This is determined by the size of these 'system clearing events' and by the rate of mass influx. In the LEM case, the largest failure event requires all hillslopes in the domain to fail into the stream channel at the same time. This can occur when landslide frequency is high but becomes less likely as landslide frequency decreases. For the moderate and low frequency scenarios, there is no transition to blue noise. It is likely that even when many landslides occur at the same time, there are always some hillslopes recovering from previous landslides. The largest events that occur over the 20-million-year experiment are not sufficiently large to clear the entire catchment.

Spectra from all scenarios exhibit a sudden increase in power at timescales above approximately 300,000 years (Figure 3). Although possibly caused by long-term rearrangement of the landscape, it is likely these are numerical artifacts.

Landscape morphology

The parameters for hillslope diffusion are set to slightly round off the ridges between drainages, but to otherwise have a minimal effect. This means that landscape morphology reflects the stronger of the two key erosive processes: landsliding and fluvial incision. When t_{LS} is high, landslides occur infrequently, so bedrock is primarily eroded by fluvial incision, resulting in short hillslopes, high drainage density, and a relatively tortuous river network. When t_{LS} is low, the landscape is dominated by long, planar hillslopes caused by frequent landsliding. The river network is direct, channel steepness is high, and relief is high as the fluvial system uses the majority of its erosive power to evacuate sediment generated by landslides. When the two processes are balanced, the landscape becomes highly dynamic as local erosive dominance shifts temporarily between the two processes.

3.5 Figures

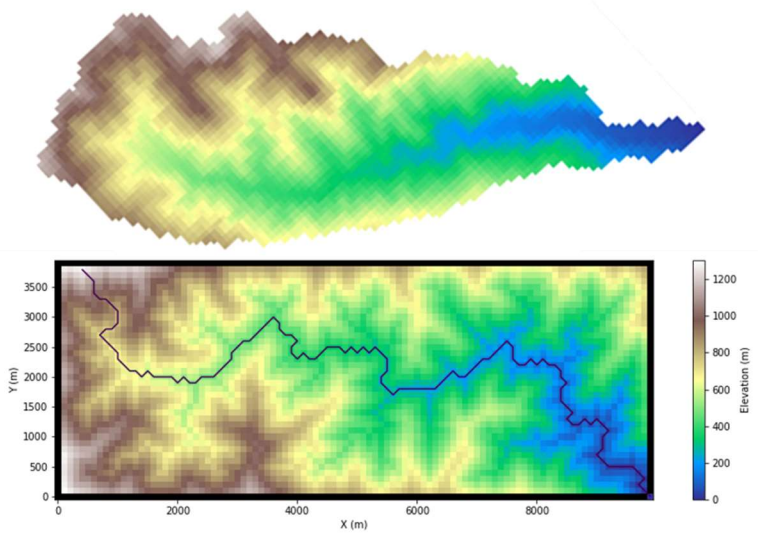

Figure 1. Comparison of the Pagliara watershed (a) and the synthetic model domain (b). Although the drainage areas differ (the synthetic watershed is 14% larger), the channel and hillslope length and steepness, drainage density, and relief are statistically similar. Note: this figure shows the model domain used for the preliminary analysis described in Section 4, which has slightly different parameters than the intended final model.

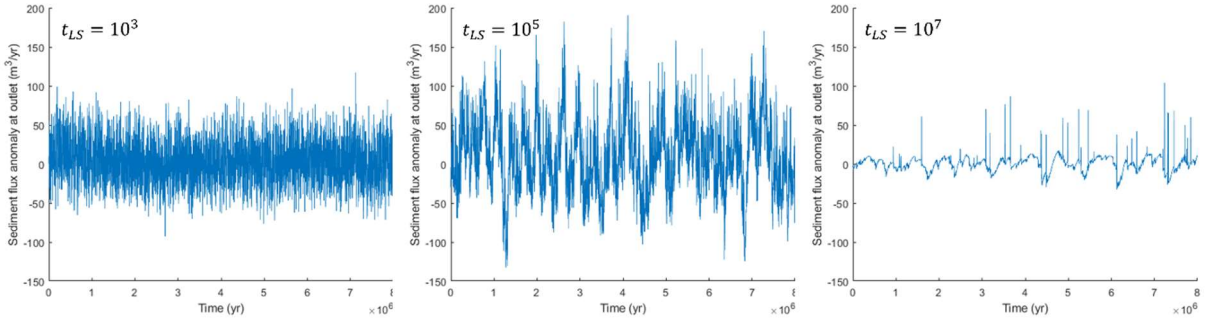

Figure 2. Timeseries of Q_s at the outlet of the catchment for three landslide return times: $t_{LS} = 10^3$ years, $t_{LS} = 10^5$ years, $t_{LS} = 10^7$ years. The x and y axes have the same scale in all three graphs.

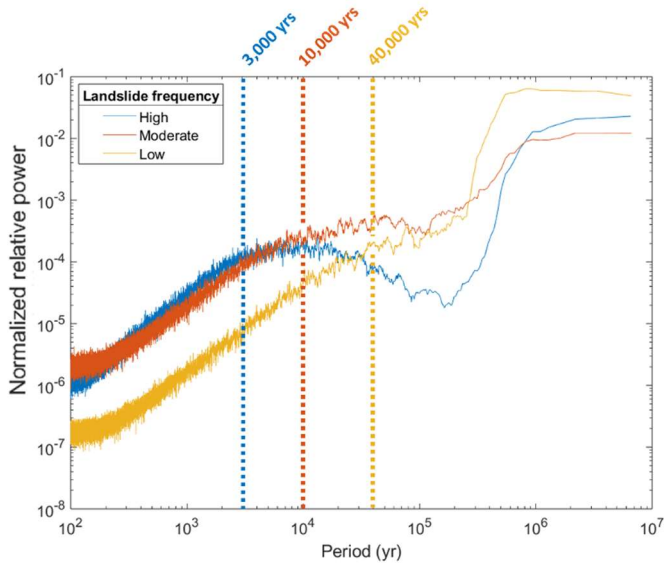

Figure 3. Spectral estimates generated using the MTM method with five DPSS tapers. The scenario with high landslide frequency (blue) shows the characteristic tripartite shape described in Griffin et al. (2023), while the moderate frequency (orange) and low frequency (yellow) scenarios do not show any blue noise at long timescales. T_{RW} shifts to longer timescales as landslide frequency decreases.

4. Project 2

Project 2 is a continuation of the modeling work from Project 1. I add exogenic tectonic forcing to the LEM to explore shredding and propagation of sedimentary signals through the erosional domain. I also add a new process component that tracks magnetic susceptibility (χ) concentrations in sediment moving across the landscape.

4.1 Introduction

Following a change in exogenic forcing, landscapes undergo a transient phase of morphologic change as they adjust to the new external state. The time it takes for this adjustment to occur is known as the response time (RT) in a detachment limited system (Whipple and Tucker, 1999; Whipple, 2001; Whipple and Tucker, 2002; Niemann et al., 2001) or the equilibrium timescale (T_{eq}) in a transport limited system (Paola et al., 1992; Allen et al., 2008; Jerolmack and Paola, 2010; Straub et al., 2020). Similarly, the sediment flux (Q_s) exiting a catchment takes some time to return to a new steady state. In response to new forcing, Q_s also exhibits a lag time (LT) before there is any sign of change. Using a detachment-limited stream power model to simulate fluvial erosion, Li et al. (2018) explored the time lag (buffering) effect of a dendritic fluvial network. In their experiment, there were no hillslope processes and once material was entrained, it was transported immediately to the outlet, allowing no chance for sediment storage on the landscape. By applying pulses of tectonic uplift of various durations, they found that the transient response of the landscape through time caused only low-frequency changes to generate Q_s signals. No signals were detectable for any rock uplift pulse shorter than 25% of the catchment's RT.

Similarly, the response of rice piles to periodic increases in input flux generates a detectable spike in the power spectra only for low frequency input signals. High-frequency signals tend to be less detectable and signals repeating over timescales shorter than T_{RW} tend to degrade in amplitude such that they cannot be detected above the background noise of the stochastic system (Griffin et al., 2023) (Figure 4). Power spectral analysis of Q_s timeseries in Project 1 shows that the interaction between the fluvial network and landslide deposits generates correlation over timescales up to a T_{RW} of 10^3 to 10^5 years. This suggests that landslides may shred sedimentary signals delivered from the erosional domain with periodicity shorter than those timescales.

However, χ may tell a different story, as it is related to the sediment's chemical composition rather than its volumetric flux. χ tends to be enhanced in soil eluvial horizons compared to the subsoil and parent bedrock material (Le Borgne, 1955; Thompson and Oldfield, 1986) due to pedogenesis (Lu et al., 2012) and preferential accumulation of weathering-resistant magnetic minerals (Singer, 1996). I intend to compare the frequency, amplitude, and phase shift of the signals carried by Q_s and by χ. Though both are transferred from hillslopes to the outlet by the same fluvial process of entrainment and transport, they may record different signals over different timescales. For example, a landslide composed mostly of bedrock may deposit the same volume of material to the valley bottom as a surficial slide composed of only soil. In both cases, the Q_s signal transported to the outlet by fluvial incision of the deposits may be the same, however the χ signal of the former deposit would be much smaller than that of the latter.

In this project, I will run a series of numerical experiments in which I add a tectonic signal to the equilibrium scenarios from Project 1. First, I will generate tectonic pulses lasting as long as the timescale T_{RW}. I will then vary the magnitude and periodicity of the pulses to explore the signal shredding

capabilities of stochastic landsliding. In addition, I will add a χ tracking component to the model, allowing me to compare the signals carried by Q_s and MS.

4.2 Hypothesis

Based on the work of Griffin et al., 2023, I hypothesize that tectonic pulses of all magnitudes that have periodicity longer than T_{RW} will be detectable as a spike in the Q_s power spectra. Those with periods shorter than T_{RW} will generate significantly degraded signals. I expect that high amplitude signals may be detectable at all timescales, but low amplitude signals may not be detectable at any timescale as they will be masked by autogenic noise. Additionally, I hypothesize that χ may carry signals from different events and over different timescales than Q_s. For example, when rock uplift rate is increased, both erosion rate and relief will rise to reach a new equilibrium state. Higher erosion rates mean higher Q_s exiting the catchment. However, increased relief should result in steeper and/or longer hillslopes that produce more and/or larger deep-seated bedrock landslides, filling the valleys with low-χ bedrock and lowering the χ signal at the outlet.

4.3 Methods

Magnetic susceptibility tracking model

I have developed a Landlab component that defines spatially variable concentrations of sediment properties and tracks them as the sediment fluxes across a numerical landscape. This component is generalized to track the concentration of any user-provided property of sediment (e.g., cosmogenic radionuclide concentration, zircon concentration, magnetic susceptibility). It works in conjunction with *SpaceLargeScaleEroder*, *BedrockLandslider*, and *DepthDependentDiffuser*. The component follows a simple mass balance approach in which property concentrations are stored prior to running each flux component and then redistributed according to the fluxes calculated by those components. In this suite of experiments, I will set the bedrock χ to 1×10^{-4} (SI units) and sediment χ to 1×10^{-3} (SI units). These values are chosen based on representative field measurements from the Pagliara watershed.

Model experiments

I will run a steady state control scenario using the same parameters as the base case from Project 1. The only difference here is the addition of the χ tracking component. I will use this scenario as a control and to characterize the differences between Q_s and MS equilibrium timeseries.

I will then add a tectonic signal by applying a sine wave to the rock uplift rates such that the minimum and maximum rates change, but the long-term rate remains the same as the control scenario. and vary the signal's period (P) relative to T_{RW} and magnitude (M) relative to the control rock uplift rate (U_c). I will run 4 iterations of different signal magnitude (M = 0.25U_c, 0.5U_c, 0.75U_c, 1U_c) across 5 different periodicities (P = 0.1T_{RW}, 0.33T_{RW}, 1T_{RW}, 3T_{RW}, 10T_{RW}) to explore the signal shredding capabilities of stochastic landsliding. These periodicities cover all three of the red, white, and blue portions of the expected power spectrum. Between pulses, rock uplift rate will be returned to U_c. Each of these 20 experiments will be run for at least 10 periods of tectonic change.

Spectral Analysis

As described in Project 1, I will use the multi-taper method for timeseries analysis. The added external forcing generates spectral peaks (Figure 4). To determine whether a spectral peak is significant compared to the background noise, the data is typically fitted with a statistical model that shows confidence levels of 90%, 95%, and 99%. Any peaks that exceed these thresholds are 'significant' and

should correspond to the imposed signal periodicity. Due to the autoregressive nature of most geological processes, the background noise is often best fit by a red noise model. Typically used are the classic or robust AR(1) log power model (Husson, 2014, or Mann and Lees, 1996, respectively), or one of the power law models following Vaughan et al. (2011). based on the results of Project 1 and of Griffin et al. (2023), it is likely that none of these approaches are adequate models of the processes modeled in this study. Instead, I will adapt the power-law model of Vaughan et al. (2011) by adding a second bend to allow the curve to fit the blue noise portion of the spectrum (Figure 5).

4.4 Results

I have not yet run the model scenarios.

4.5 Significance

This project expands on the recent research of Griffin et al. (2023) showing that avalanching rice piles generate a red-white-blue noise structure over key autogenic timescales. The results of my experiments will confirm whether the red-white-blue noise structure is generalizable to coupled systems of multiple interacting processes. The results will also provide a better understanding of the signal shredding capabilities of the red, white, and blue noise portions of the power spectra. Through these experiments, I will help define the types of environmental signals one can expect to resolve in sediment fluxes leaving erosional catchments. This will improve our ability to reconstruct Earth History and our ability to understand the situations in which that history cannot survive the autogenic noise of an erosional catchment.

Additionally, I will provide insight into whether the magnetic property χ may be related to upstream earth surface processes and into how this property may (or may not) provide information over timescales that cannot be resolved by volumetric measurements of sediment alone.

4.6 Figures

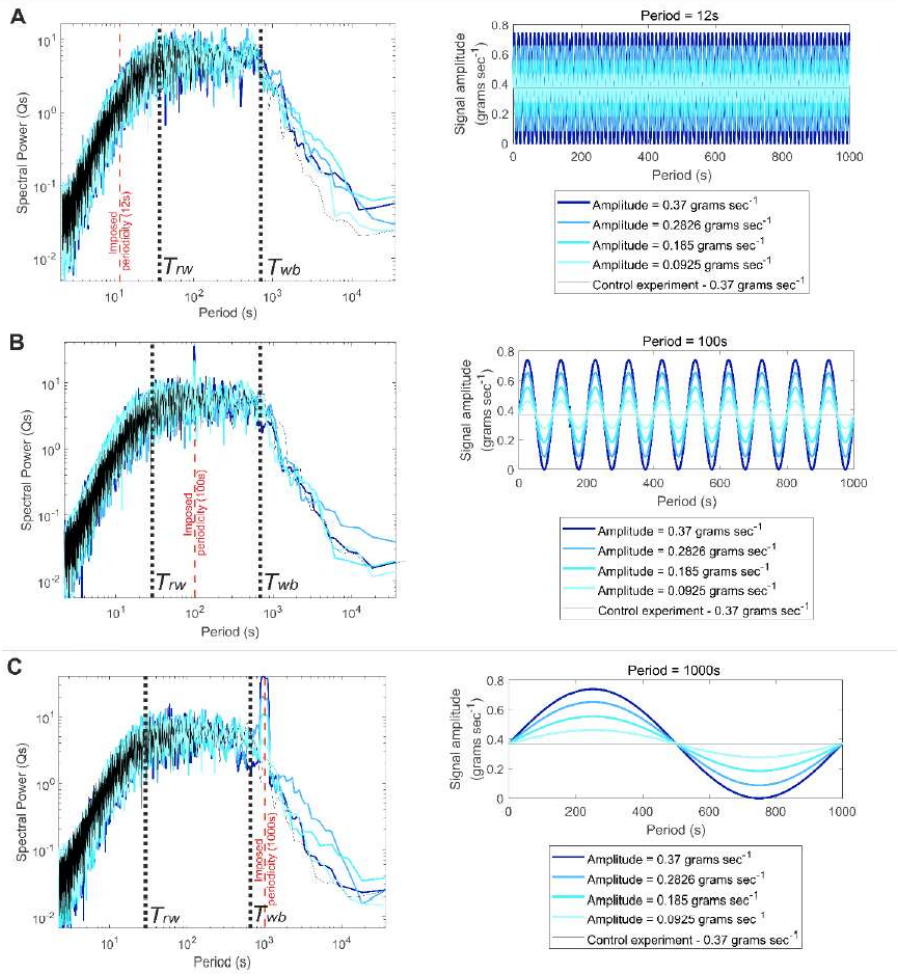

Figure 4. Example of power spectral spikes caused by imposed signals from periodic oscillations in input feed rate for rice pile models. A) shows that signals with periodicity at timescales smaller than T_{RW} are undetectable compared to background noise. B) and C) show spikes that increase in detectability as signal amplitude is increased for periodicities in the white noise and blue noise portions of the spectra, respectively. Figure from Griffin et al. (2023).

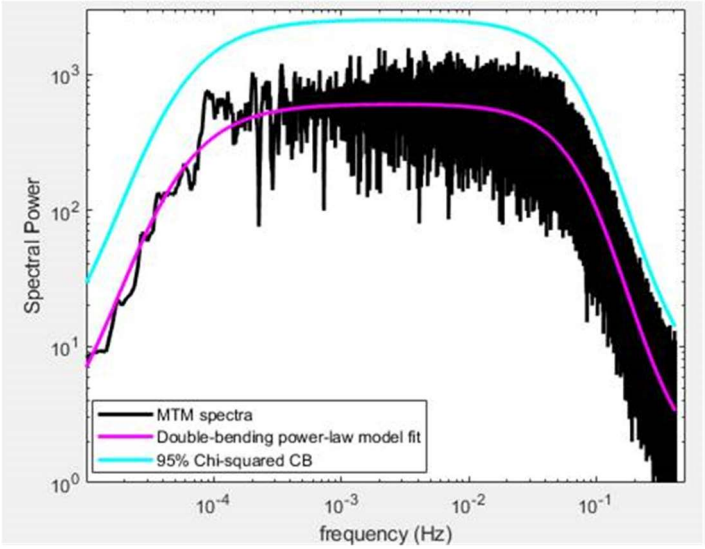

Figure 5. Example of the double-bending power law (pink line) adapted from Vaughan et al. (2011) applied to a power spectrum from a rice pile model. Figure from Kyle Straub.

5. Project 3

Project 3 is an exploration of noise transfer across sediment routing system domains using physical experiments. I will use the understanding of noise structure, magnitudes, and timescales gained from Projects 1 and 2 to inform the experimental designs.

5.1 Introduction

The sediment routing system is a conveyer belt that moves sediment from one process domain to another. Research on the depositional domain has generated robust understanding of the various autogenic processes in sedimentary basins (Hajek and Straub 2017). However, this research tends to assume sediment delivery (Q_{in}) from upstream is steady or follows simple periodic oscillations [e.g., Jerolmack and Paola, 2010; Griffin et al., 2023; Foreman and Straub, 2017). This is unlike the sporadic and unsteady delivery that occurs in natural systems. Noise in this delivery process might still have structure (i.e., correlated noise) from inheritance of prior conditions. An example is the red-to-white-to-blue noise structure of avalanching rice and sand piles (Jerolmack and Paola, 2010; Pradhan, 2021; Griffin et al., 2023), which might be generalizable to many earth surface processes. Griffin et al. (2023) theorize that a key timescale exists (T_{RW}) that separates correlated (red) from uncorrelated (white) noise, below which propagating environmental signals get significantly degraded. One of the questions that remains to be answered is how noisy delivery of sediment to a system (e.g., landsliding) interacts with the noise generated by mass transport to alter key timescales such as T_{RW}.

Depositional basins are recorders of earth history and are used to understand past environments and predict Earth's future. However, signals must first survive propagation in sediment routing systems prior to deposition (Straub et al., 2020). I will use a series of physical rice pile experiments with specifically structured noisy input flux (Q_{in}) timeseries to investigate noise transfer through a stochastic mass flux system. Q_{in} will be structured to have timescales T_{RW}^{in} and T_{WB}^{in} different to the autogenic timescales of the rice pile itself ($T_{RW}^{control}$ and $T_{WB}^{control}$) determined by the control experiments from Griffin et al. (2023). The experiments will test whether correlated noise entering a sediment transport segment is transferred down system to be measured in the output flux (Q_{out}) and seen in its key output timescales T_{RW}^{out} and T_{WB}^{out}. I explicitly differentiate between the control experiment timescales ($T_{RW}^{control}$ and $T_{WB}^{control}$) and the output timescales from these experiments (T_{RW}^{out} and T_{WB}^{out}) in case these timescales are not purely inherent to the system, but affected by input noise. The results will inform a physical delta experiment investigating the same concept to confirm whether the rice pile results can be generalized to other sediment transport systems. These experiments are intended to answer the questions: Does noisy sediment input change the autogenic behaviour of stochastic mass flux systems? What noise signatures and timescales transfer from one domain of the sediment routing system to the next?

5.2 Hypothesis

Like cyclical changes to Q_{in}, I expect stochastic variation of Q_{in} to alter delta dynamics and produce results that differ from steady feed conditions. I hypothesize that correlation in noisy Q_{in} will transfer to measurable correlation in output flux only at timescales longer than the internal T_{RW} of the system ($T_{RW}^{control}$). In other words, T_{RW}^{in} entering a segment of the sediment routing system will only transfer across the segment to be seen in T_{RW}^{out} if it occurs over timescales longer than $T_{RW}^{control}$ (Figure 7).

5.3 Methods

The experiments will be conducted at the Tulane University Sediment Dynamics and Stratigraphy Laboratory, where there is infrastructure for rice pile and delta basin experiments (Figure 6). Equipment, power, and water are supplied by the laboratory. Infrastructure in-place includes an automated high-precision sediment feeder and scale, software to automate water and sediment delivery, and a LiDAR system to collect high-precision topography and co-registered images. Facilities have been calibrated and previous experiments with steady Q_{in} will serve as controls (Griffin et al., 2023; Straub et al., 2015).

I will run six rice pile experiments to guide magnitude and timescale requirements of input sediment fluxes for the delta experiment. The first three experiments will test Q_{in} characterized only by white, by red, and by blue noise, respectively. The next three will test Q_{in} containing different T_{RW}^{in} values: a short value (1/4 of $T_{RW}^{control}$), moderate value (equal to $T_{RW}^{control}$), and long value (four times $T_{RW}^{control}$). Although Q_{in} will be noisy, the long-term average Q_{in} will be equal to that of the steady-feed control experiments. I will run multiple realizations of each experiment.

The delta basin experiment will focus on different T_{RW}^{in} values compared to a known compensation timescale (T_c, equal to 50 hrs) of the control experiment (Li et al., 2016). T_c is assumed to be analogous to $T_{WB}^{control}$ from the rice pile experiments (Griffin et al., 2023). As with the rice pile, I will run a short T_{RW}^{in} (1/4 of the delta's T_c), moderate T_{RW}^{in} (equal to T_c), and long T_{RW}^{in} (four times T_c) (Figure 7). Given the system's T_c, experimental run time will be 900 hrs to generate timeseries sufficient for spectral analysis. The long-term Q_{in} will be equal to that of the control experiment (Li et al., 2016). The water flux input will remain constant. The experiment will evolve under a constant rate of sea-level rise to simulate spatially uniform long-term subsidence that generates accommodation equal to the long-term Q_{in} (Straub et al., 2015). A terrestrial LiDAR scan and overhead image will be captured every hour. Blue dye will be injected into the water prior to imaging to help distinguish channels. The topographic scans will be differenced after the experiment to generate synthetic stratigraphy (Strong and Paola, 2008) and calculate mass flux timeseries that will be analyzed for its spectral structure. The grain size mixture will have a wide distribution (1-1000 µm, and D50 = 67 µm), with an additive to enhance deposit cohesion.

Budget

I will use play sand to create a smooth substrate surface on top of which the delta experiment is performed. I will then use various quartz sediments to produce a wide distribution mixture to generate synthetic stratigraphy. After the experiment, I will cover the deposit with more play sand to prevent moisture loss and cracking. Sediment volumes are based on previous experiments in the same delta basin. Prices are from http://tsmaterials.com/products/ and https://www.acehardware.com.

Equipment maintenance:	**$1,000**
Dye:	**$250**
Play sand (40 sacks):	**$320**
	40 sacks (50lb each). $8/sack
Quartz sediments (255 sacks):	**$5,175**
120 Mesh Silica Sand	75 sacks (50lb each). $21/sack
WF-1 fine sieved	75 sacks (50lb each). $21/sack
Kosse industrial 18/100 Dry	75 sacks (50lb each). $27/sack
Total cost:	**$6,745**

5.4 Results

I have not yet run the experiments.

5.5 Significance

This project will increase our understanding of signal propagation across landscapes. I expect the rice pile and delta experiments to generate analogous results and show that the red-white-blue noise framework applies to multiple experimental processes. This will build confidence to use it for interpreting the stratigraphic record. Given understanding of upstream processes, I will develop theory to better extract time-varying signals from strata, to better invert stratigraphy for past climate or tectonic changes, and to better understand responses to future perturbations.

5.6 Figures

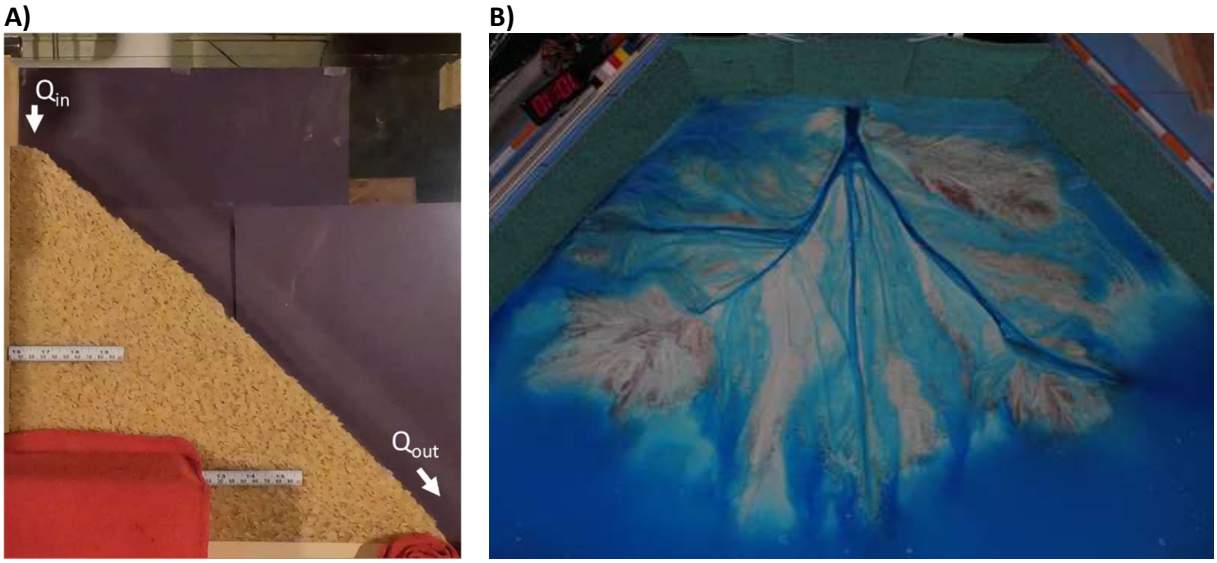

Figure 6. Example of A) a rice pile experiment and B) a delta experiment at the Tulane University Sediment Dynamics and Stratigraphy Laboratory. Images from Kyle Straub.

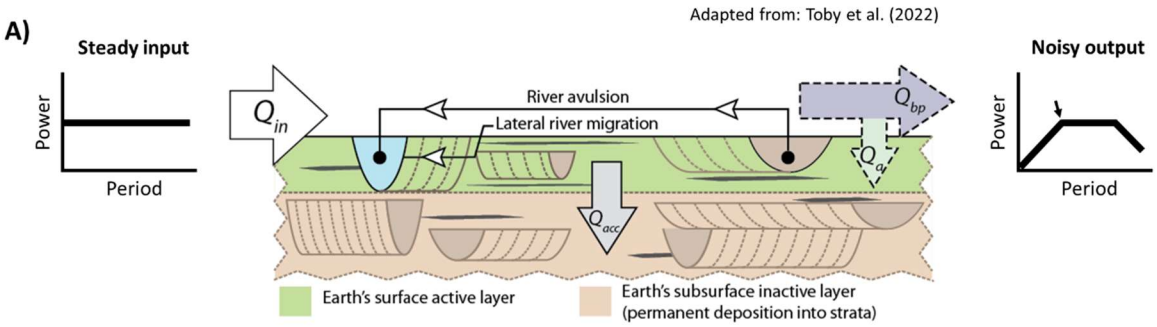

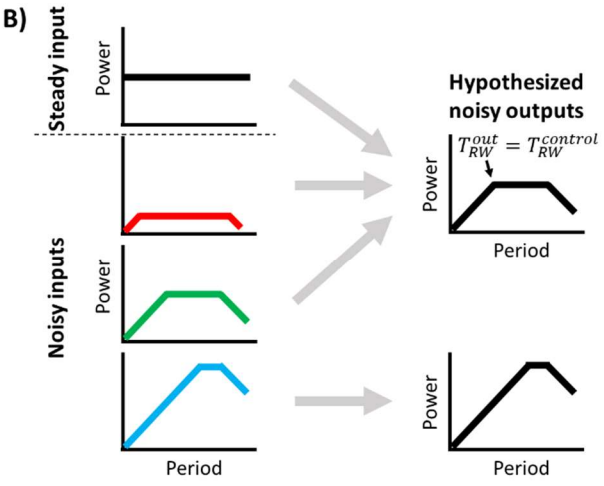

Figure 7.

A) Example segment of a sediment routing system. Steady sediment delivery (Q_{in}) is shown as a horizontal line on a periodogram. Some sediment is permanently deposited into strata (Q_{acc}), some is temporarily deposited in the active layer where remobilization by autogenic processes such as river avulsion and migration is possible (Q_a), and some bypasses the segment either directly or after temporary deposition and remobilization (Q_{bp}). The result is noisy sediment flux out of the segment, shown with characteristic red-white-blue noise structure. The transition from red to white noise (T_{RW}) separates correlated (red) from uncorrelated (white) noise, below which propagating environmental signals become significantly degraded.

B) Conceptual schematic of inputs and hypothesized outputs for the delta basin experiment. The noisy inputs have a T_{RW}^{in} shorter (red), equal (green), and longer (blue) than that of the delta's control experiment ($T_{RW}^{control}$). I expect input noise structures existing at timescales shorter than or equal to $T_{RW}^{control}$ (red and green inputs) to be overprinted by the delta's autogenic processes, resulting in outputs indistinguishable from that of a steady input, while input noise structures existing at timescales longer than $T_{RW}^{control}$ (blue) will survive to produce a measurably different output flux.

8. References

Allen, P. A. (2008). Time scales of tectonic landscapes and their sediment routing systems. In K. Gallager, S. J. Jones, & J. Wainwright (Eds.), Landscape evolution: Denudation, climate and tectonics over different time and space scales (pp. 7–28). London.

Armitage, J.J., Duller, R.A., Whittaker, A.C., and Allen, P.A. (2011,).Transformation of tectonic and climatic signals from source to sedimentary archive: Nature Geoscience, v. 4, p. 231–235, https://doi.org/10.1038/ngeo1087.

Barnhart, K. R., Hutton, E. W. H., Tucker, G. E., M. Gasparini, N., Istanbulluoglu, E., E. J. Hobley, D., J. Lyons, N., Mouchene, M., Siddhartha Nudurupati, S., M. Adams, J., and Bandaragoda, C. (2020). Short communication: Landlab v2.0: A software package for Earth surface dynamics. Earth Surface Dynamics, 8(2), 379–397. https://doi.org/10.5194/esurf-8-379-2020

Barnhart, K.R., Glade, R.C., Shobe, C.M., and Tucker, G.E. (2019). Terrainbento 1.0: a Python package for multi-model analysis in long-term drainage basin evolution. Geoscientific Model Development, 12, 1267 – 1297. https://doi.org/10.5194/gmd-12-1267-2019

Campforts, B., Shobe, C.M., Steer, P., Vanmaercke, M., Lague, D., and Braun, J. (2020). HyLands 1.0: a hybrid landscape evolution model to simulate the impact of landslides and landslide-derived sediment on landscape evolution. Geosci. Model Dev. 13, 3863–3886, https://doi.org/10.5194/gmd-13-3863-2020

Campforts, B., Shobe, C.M., Overeem, I., and Tucker, G.E. (2022). The Art of Landslides: How Stochastic Mass Wasting Shapes Topography and Influences Landscape Dynamics. JGR Earth Surface 127(8), https://doi.org/10.1029/2022JF006745

Catalano, S. and De Guidi, G. (2003). Late quaternary uplift of northeastern Sicily: relation with the active normal faulting deformation. J. Geodyn. 36, 445–467.

Castelltort, S., and Van Den Driessche, J. (2003). How plausible are high-frequency sediment supply-driven cycles in the stratigraphic record? Sedimentary Geology, 157, 3–13, https://doi.org/10.1016/S0037-0738(03)00066-6

Crave, A., and Davy, P. 2000. A stochastic ‘‘precipiton’’ model for simulating erosion/sedimentation dynamics. Computers & Geosciences. 27: 815–827.

Cyr, A.J., Granger, D.E., Olivetti, V., and Molin, P. (2010). Quantifying rock uplift rates using channel steepness and cosmogenic nuclide-determined erosion rates: examples from northern and southern Italy. Lithosphere 2, 188–198. http://dx.doi.org/10.1130/L96.1

Foreman, B.Z. and Straub, K.M. (2017). Autogenic geomorphic processes determine the resolution and fidelity of terrestrial paleoclimate records. Sci. Adv. 3(9), e1700683. DOI: 10.1126/sciadv.1700683

Forzoni, A., Storms, J.E., Whittaker, A.C., and Jager, G. (2014). Delayed delivery from the sediment factory: Modeling the impact of catchment response time to tectonics on sediment flux and fluvio-deltaic stratigraphy: Earth Surface Processes and Landforms, v. 39, p. 689–704, https://doi.org/10.1002/esp.3538.

Gasparini, N. M., Whipple, K. X., & Bras, R. L. (2007). Predictions of steady state and transient landscape morphology using sediment-flux-dependent river incision models. Journal of Geophysical Research: Earth Surface, 112(3), 1–20. https://doi.org/10.1029/2006JF000567

Godard, V., Tucker, G.E., Fisher, G.B., Burbank, D.W., and Bookhagen, B. (2013). Frequency-dependent landscape response to climatic forcing. Geophys. Res. Lett., 40, 859–63.

Goren, L., Willett, S. D., Herman, F., and Braun, J. 2014. Coupled numerical-analytical approach to landscape evolution modeling. Earth Surf. Process. Landforms. 39, 522–545 (2014)

Goswami, R., Brocklehurst, S.H., and Mitchell, N.C. (2012). Erosion of a tectonically uplifting coastal landscape, NE Sicily, Italy: Geomorphology, v. 171–172, p. 112–126, doi: 10.1016/j.geomorph.2012.05.011.

Griffin, C., Duller, R. A., and Straub, K. M. (2023). The degradation and detection of environmental signals in sediment transport systems. Science Advances, in press.

Hajek, E.A. and Straub, K.M. (2017). Autogenic Sedimentation in Clastic Stratigraphy. Annu. Rev. Earth Planet. Sci. 45: 681–709. https://doi.org/10.1146/annurev-earth-063016-015935

Hobley, D. E. J., Adams, J. M., Nudurupati, S. S., Hutton, E. W. H., Gasparini, N. M., Istanbulluoglu, E., and Tucker, G. E. (2017). Creative computing with Landlab: an open-source toolkit for building, coupling, and exploring two-dimensional numerical models of Earth-surface dynamics. Earth Surf. Dynam., 5, 21–46. https://doi.org/10.5194/esurf-5-21-2017

Husson, D. (2014). MathWorks File Exchange: RedNoise_ConfidenceLevels, https://www.mathworks.com/matlabcentral/fileexchange/45539-rednoise_confidencelevels with corrections by L.A. Hinnov.

Hwa, T., and Kardar, M. (1992). Avalanches, hydrodynamics, and discharge events in models of sandpiles. Physical Review A, 45(10), 7002–7023.

Jerolmack, D. J., and Paola, C. (2010). Shredding of environmental signals by sediment transport. Geophysical Research Letters, 37(19), 1–5. https://doi.org/10.1029/2010GL044638

Le Borgne, E. (1955). Susceptibilité magnétique anormal de sol superficial. Annals of Geophysics, 11, 399--419.

Lentini, F., Catalano, S., and Carbone, S. (2000). Nota illustrativa della Carta geologica della Provincia di Messina (Sicilia Nord-Orientale): Firenze, Società Elaborazioni Cartografiche (S.EL.CA.), scale 1:50,000, 70 p.

Li, M., Hinnov, L.A., and Kump, L.R. (2019). Acycle: Time-series analysis software for paleoclimate projects and education, Computers and Geosciences, 127: 12-22. https://doi.org/10.1016/j.cageo.2019.02.011

Li, Q., Yu, L., and Straub, K. M. (2016). Storage thresholds for relative sea-level signals in the stratigraphic record. Geology, 44(3). https://doi.org/10.1130/G37484.1

Li, Q., Gasparini, N. M., and Straub, K. M. (2018). Some signals are not the same as they appear: How do erosional landscapes transform tectonic history into sediment flux records? Geology, 46(5), 407–410. https://doi.org/10.1130/G40026.1

Lu, S.G., Chen, D.J., Wang, S.Y. & Liu, Y.D., 2012. Rock magnetism investigation of highly magnetic soil developed on calcareous rock in Yun-Gui Plateau, China: Evidence for pedogenic magnetic minerals, J. appl. Geophys., 77, 39–50.

Mann, M.E., and Lees, J.M. (1996). Robust estimation of background noise and signal detection in climatic time series. Climatic Change, 33, 409-445, https://doi.org/10.1007/BF00142586.

Niemann, J.D., Gasparini, N.M., Tucker, G.E., and Bras, R.L. 2001. A quantitative evaluation of Playfair's Law and its use in testing long-term stream erosion models . Earth Surf. Process. Landforms 26, 1317–1332

Paola, C., Heller, P. L., & Angevine, C. L. (1992). The large-scale dynamics of grain-size variation in alluvial basins. 1: Theory. Basin Research, 4, 73–90.

Pavano, F., Pazzaglia, F.J., and Catalano, S. (2016). Knickpoints as geomorphic markers of active tectonics: a case study from northeastern Sicily (southern Italy). Lithosphere-US 8 (6):633–648. https://doi.org/10.1130/L577.1

Perron, J. T., Kirchner, J. W., & Dietrich, W. E. (2009). Formation of evenly spaced ridges and valleys. Nature, 460(7254), 502–505. https://doi.org/10.1038/nature08174

Phillips, C. B., and Jerolmack, D. J. (2016). Self-organization of river channels as a critical filter on climate signals. Science, 352(6286), 694–697. https://doi.org/10.1126/science.aad3348

Pizzuto, J., Keeler, J., Skalak, K., and Karwan, D. (2017). Storage filters upland suspended sediment signals delivered from watersheds. Geology, 45, 151–154, https://doi.org/10.1130/G38170.1

Pradhan, P. (2021). Time-Dependent Properties of Sandpiles. Frontiers in Physics, 9:641233. https://doi.org/10.3389/fphy.2021.641233

Roda-Boluda, D.C., D'Arcy, M., McDonald, J. and Whittaker, A.C. (2018) Lithological controls on hillslope sediment supply: Insights from landslide activity and grain size distributions. Earth Surface Processes and Landforms, 43(5), 956–977. https://doi.org/10.1002/esp.4281

Romans, B.W., Castelltort, S., Covault, J.A., Fildani, A., and Walsh, J. (2016). Environmental signal propagation in sedimentary systems across timescales: Earth-Science Reviews, v. 153, p. 7–29, https://doi.org/10.1016/j.earscirev.2015.07.012.

Sharman, G. R., Sylvester, Z., and Covault, J. A. (2019). Conversion of tectonic and climatic forcings into records of sediment supply and provenance. Scientific Reports, 9(1), 1–7. https://doi.org/10.1038/s41598-019-39754-6

Shobe, C. M., Tucker, G. E., and Barnhart, K. R. (2017). The SPACE 1.0 model: A Landlab component for 2-D calculation of sediment transport, bedrock erosion, and landscape evolution. Geoscientific Model Development, 10(12), 4577–4604. https://doi.org/10.5194/gmd-10-4577-2017

Singer, M.J., Verosub, K.L., Fine, P., and TenPas, J. (1996). A conceptual model for the enhancement of magnetic susceptibility in soils, Quat. Int., 34–36 (1996), pp. 243-248, 10.1016/1040-6182(95)00089-5

Straub, K. M., Li, Q., and Benson, W. M. (2015). Influence of sediment cohesion on deltaic shoreline dynamics and bulk sediment retention: A laboratory study. Geophysical Research Letters, 42. https://doi.org/10.1002/2015GL066131

Straub, K. M., Duller, R. A., Foreman, B. Z., and Hajek, E. A. (2020). Buffered, Incomplete, and Shredded: The Challenges of Reading an Imperfect Stratigraphic Record. Journal of Geophysical Research: Earth Surface, 125(3), 1–44. https://doi.org/10.1029/2019JF005079

Strong, N., and Paola, C. (2008). Valleys that never were: Time surfaces versus stratigraphic surfaces. Journal of Sedimentary Research, 78(8), 579–593. https://doi.org/10.2110/jsr.2008.059

Thomson, D.J. (1982). Spectrum estimation and harmonic analysis. Proceedings of the IEEE 70, 1055-1096.

Thompson, M. and Oldfield, F. (1986). Environmental Magnetism. Allen and Unwin, London.

Toby, S.C., Duller, R.A., De Angelis, S., and Straub K.M. (2022). Morphodynamic limits to environmental signal propagation across landscapes and into strata. Nat Commun 13, 292. https://doi.org/10.1038/s41467-021-27776-6

Toonen, W. H. J., Foulds, S. A., Macklin, M. G., and Lewin, J. (2017). Events, episodes, and phases: Signal from noise in flood-sediment archives. Geology, 45(4), 331–334. https://doi.org/10.1130/G38540.1

Trampush, S. M., and Hajek, E. A. (2017). Preserving proxy records in dynamic landscapes: Modeling and examples from the Paleocene-Eocene Thermal Maximum. Geology, 45(11), 967–970.

Tucker, G. E., & Bras, R. L. (1998). Hillslope processes, drainage density, and landscape morphology. Water Resources Research, 34(10), 2751–2764.

Tucker, G. E., & Bras, R. L. (2000). A stochasticapproach to modeling the role of rainfall variability in drainage basin evolution. Water Resources Research, 36(7), 1953–1964.

Vaughan, S., Bailey, R., and Smith, D. (2011). Detecting cycles in stratigraphic data: Spectral analysis in the presence of red noise. Paleoceanography 26.

Weedon, G.P. (2003.) Time Series Analysis and Cyclostratigraphy: Examining Stratigraphic Records of Environmental Cycles. Cambridge University Press, pp. 259.

Whipple, K.X, and Tucker, G.E. (1999). Dynamics of the stream-power river incision model: Implications for height limits of mountain ranges, landscape response timescales, and research needs: Journal of Geophysical Research: Solid Earth, v. 104, B8, p. 17661–17674, https://doi.org/10.1029/1999JB900120.

Whipple, K. X., and Tucker, G.E. (2002). Implications of sediment-flux-dependent river incision models for landscape evolution. Journal of Geophysical Research, 107(B2). https://doi.org/10.1029/2000jb000044
Whipple, K.X. (2001). Fluvial landscape response time: How plausible is steady state denudation? American Journal of Science, v. 301, p. 313–325, https://doi.org/10.2475/ajs.301.4-5.313.

Willgoose, G., Bras, R. L., & Rodriguez-Iturbe, I. (1991). A coupled channel network growth and hillslope evolution model: 1. Theory. Water Resources Research, 27(7), 1671–1684.